

Preparation and Characterization of Outdoor Bamboo-Fiber-Reinforced Composites with Different Densities

Fei Rao,^{a,c} Yuhe Chen,^{a,c,*} Neng Li,^{a,c,*} Xiping Zhao,^b Yongjie Bao,^{a,c} Zaixing Wu,^{a,c} Danjing Ren,^{a,c} Jun Xu,^{a,c} and Hanjiang Cai^a

Outdoor bamboo-fiber-reinforced composites (OBFRCs) with four different densities were prepared, and the microstructure and physicomechanical properties of pristine samples were evaluated. In addition, the surface color, glossiness, roughness, water absorption, and wettability of the samples were tested to investigate the effects of panel density on the extent of surface weathering due to ultraviolet radiation. The results showed that the OBFRCs exhibited excellent physical and mechanical properties, which improved with increasing density. However, increases in the density led to decreases in the hygroscopicity and dimensional stability of the OBFRCs. After weathering, the surface contact angle and surface roughness increased, and the dimensional stability improved. The surface glossiness, water absorption, and surface free energy decreased. A higher density resulted in improved color stability, which suggested that density played an important role in determining surface photodegradation properties. Thus, density-increasing treatments had positive effects on the physical and mechanical properties as well as the color stability and wettability of the OBFRCs, but they may negatively affect the roughness and dimensional stability. Based on service-performance and cost-minimization considerations, 1.1 g/cm³ was determined as the most appropriate density for general applications.

Keywords: Outdoor bamboo-fiber-reinforced composites; Density; Weathering; Surface Properties

Contact information: a: China National Bamboo Research Center, Hangzhou 310012, China; b: Forestry College, Henan University of Science and Technology, Luoyang 471000, China; c: Key Laboratory of High Efficient Processing of Bamboo of Zhejiang Province, Hangzhou 310012, China;

* Corresponding authors: yuhec@sina.com; lineng8657@sina.com

INTRODUCTION

Bamboo is a sustainable ecological material that can be equivalent in structural value to wood (Tomak *et al.* 2012). It is used extensively for making furniture, flooring, pulp, and paper, *etc.*, due to its attractive natural color, elegant texture, cultural value, ease of processing, and high strength-to-weight ratio (Wang and Ren 2008). Technologies for fabricating high-performance bamboo-fiber-reinforced composites (BFRCs) help overcome the inherent defects of bamboo, such as its small diameter and thin walls. Processes for making BFRCs can also improve the bonding between the outer and inner bamboo culms and improve the utilization of bamboo veneer for panel production (Yu *et al.* 2014; Zhu *et al.* 2015). The next step in the development of BFRCs is to improve their outdoor performance, which will ease the demand for wood resources and take advantage of the availability of bamboo. When bamboo is exposed to outdoor weathering conditions such as solar radiation, moisture, oxygen, high temperatures,

bacteria, or fungus, the exterior becomes discolored, and it loses its glossiness. In addition, its strength and adhesive capabilities are reduced; it becomes rougher and exhibits chalking (Hayoz *et al.* 2003; George *et al.* 2005; Pandey 2005; Cristea *et al.* 2010; Chaochanchaikul *et al.* 2013).

The photodegradation of bamboo under outdoor weathering conditions depends on several factors such as the water content, whether the material has been subjected to a thermal or chemical modification treatment, its density, and the surrounding environmental conditions. It was reported that reducing the moisture content of wood is a good way to protect it against weathering (Weichelt *et al.* 2011). According to Lesar *et al.* (2011), a wax treatment can retard weathering to a certain extent due to the hydrophobicity of the treated wood. Furthermore, a thermal treatment can significantly improve the color stability of wood. However, thermal treatment also degrades its natural color and strength (Shangguan *et al.* 2016; Yang *et al.* 2016). To counteract this effect, the lignin phenoxy radicals of acetylated wood have been used with some success in reducing photoinduced degradation and improving the dimensional stability of wood (Beckers *et al.* 1998). Coating the exposed surfaces with inorganic and organic ultraviolet (UV) radiation absorbers is another option (Zhu *et al.* 2008; Li *et al.* 2015). The higher density of these products makes it difficult for water and light to reach the wood (Kataoka *et al.* 2005). The depth of the photodegradation and the rate of erosion of the wood during weathering depends greatly on the density (Horn *et al.* 1994; Evans *et al.* 2005). Many previous studies of anti-aging treatments have focused on the changes in the physical and mechanical properties, color characteristics, and chemical composition of bamboo and bamboo-based composites (Beckers *et al.* 1998; Cristea *et al.* 2010; Lesar *et al.* 2011; Tolvaj *et al.* 2011; Srinivas and Pandey 2012; Tomak *et al.* 2012; Baysal *et al.* 2014; Tolvaj *et al.* 2014; Li *et al.* 2015; Zhu *et al.* 2015; Shangguan *et al.* 2016). Furthermore, the effects of the density on the performance of bamboo and bamboo-based composites have been reported (Evans *et al.* 2005; Tolvaj *et al.* 2011; Srinivas and Pandey 2012; Baysal *et al.* 2014; Tolvaj *et al.* 2014; Li *et al.* 2017).

In this study, high-durability outdoor bamboo-fiber-reinforced composites (OBFRCs) with four different densities were produced to investigate the effects of the density on the weathering characteristics of the composites. In addition, this study aimed to determine the correlations between the density of the various panels and their water resistance, surface wettability, color stability, and chemical composition during accelerated weathering. Microscopic structural analyses were performed using scanning electron microscopy (SEM). The mechanical and physical properties were evaluated in terms of the modulus of rupture (MOR), modulus of elasticity (MOE), horizontal shear strength (HS), water absorption rate (WAR), and volume swelling efficiency (VSE). The wettability was evaluated through contact angle (CA) measurements and surface free energy (SFE) calculations. The changes in the color of the exposed surfaces were investigated using the CIELAB color system

EXPERIMENTAL

Materials

Preparation of outdoor bamboo-fiber-reinforced composites (OBFRCs)

The OBFRCs were prepared according to the standard procedure (Yu *et al.* 2014), as shown in Fig. 1. Four-year-old moso bamboo (*Phyllostachys pubescens* Mazel) culms

were harvested at a plantation located in Anhui province in eastern China. Each 5 mm to 6 mm culm was split longitudinally into two semicircular parts, and the edges were trimmed into 450 mm long pieces.

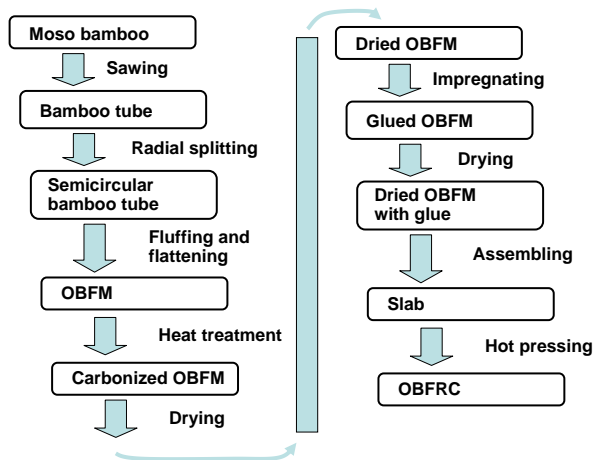


Fig. 1. Process for fabricating OBFRCs

Net-like oriented bamboo-fiber mats (OBFMs) were formed by fluffing and flattening the fibers along their longitudinal axis. The mats were then oven dried to ensure a moisture content of 6% to 8% (w/w). The OBFMs were then subjected to vapor pressure as a medium for heat treatment for 2 h at 121.8 °C to 128.7 °C. The carbonized OBFMs were soaked in a 20% (w/w) phenol formaldehyde resin (PF) solution for approximately 5 min to achieve a resin content of 14% (w/w). The original undiluted PF had a solid content of 46.2% (w/w), viscosity of 36 mPa·s at 23 °C, and pH of 10 to 11 (Beijing Taier Chemical Co., Ltd., Beijing, China). Equation 1 was used to calculate the resin content of the OBFMs,

$$C = \frac{(m_2 - m_1) \times w}{m_1 \times (1 - x)} \quad (1)$$

where C is the resin content; m_1 and m_2 are weights of the OBFM in question pre- and post-immersion in the resin, respectively; w is the solid content of the resin; and x is the wet-basis moisture content of the OBFM pre-immersion in the resin. After immersion in PF, the OBFMs were oven-dried at 55 °C until they had a moisture content of 11 to 12%.

Table 1. Measured Densities of Pristine and Weathered Samples

Sample	SEM	WA/VSE	MOR/MOE	HS	Color	CA/SFE	
Pristine	A _o	0.91	0.86(0.006)	0.90(0.020)	0.90(0.020)	0.90(0.019)	0.91(0.018)
	B _o	1.00	1.00(0.011)	0.98(0.018)	0.99(0.040)	0.99(0.013)	0.98(0.019)
	C _o	1.11	1.10(0.007)	1.10(0.030)	1.10(0.025)	1.09(0.013)	1.10(0.035)
	D _o	1.21	1.20(0.034)	1.17(0.011)	1.17(0.012)	1.17(0.006)	1.17(0.013)
Weathered	A _w	—	0.85(0.005)	—	—	0.90(0.019)	0.90(0.016)
	B _w	—	1.00(0.017)	—	—	0.99(0.013)	0.98(0.017)
	C _w	—	1.11(0.027)	—	—	1.09(0.013)	1.08(0.015)
	D _w	—	1.21(0.044)	—	—	1.17(0.006)	1.17(0.010)

Note: The letters A, B, C, and D represent the four densities (0.9 g/cm³, 1.0 g/cm³, 1.1 g/cm³, and 1.2 g/cm³, respectively), while the subscripts o (original) and w (weathered) represent the pristine and weathered specimens. Standard deviation is shown in parentheses.

The designed densities of 0.9 g/cm³ to 1.2 g/cm³ were achieved by controlling the weight of the resin-impregnated OBFMs after drying. All of the weighed mats were assembled symmetrically along the grain, with the outer layer being outward and the inner surface being inward, such that they could be laid evenly and loosely to form slabs. The slabs were transferred to a single-opening hydraulic hot press (QD, Shanghai Artificial Board Machinery Factory Co., Ltd., Shanghai, China) for hot-pressing, which was performed using the cold-in and cold-out technique. During the process, the slabs were pressed at a hot-plate temperature of 145 °C for a holding time of 1 min/mm and unloaded at a hot-plate temperature between 55 °C and 66 °C. This resulted in a slab thickness of 20 mm. Finally, OBFRCs with target densities of 0.90 g/cm³ to 1.20 g/cm³ were obtained by cutting the edges of the samples and sanding them. All samples were conditioned in a controlled-environment room at 20 °C and relative humidity (RH) of 65% for 2 weeks before being tested. Depending on the test and analysis requirements, samples of different dimensions were cut and marked. The letters A, B, C, and D represent the four densities (0.9 g/cm³, 1.0 g/cm³, 1.1 g/cm³, and 1.2 g/cm³, respectively), while the subscripts o (original) and w (weathered) represent the pristine and weathered specimens. The measured densities of the pristine (original) and weathered samples are listed in Table 1.

Methods

Accelerated UV weathering test

The samples were fixed in stainless steel holders and subjected to irradiation by a fluorescent UV-visible light (UVB-313 lamp, 0.71 W/m²) using an accelerated UV weathering test box (Hangzhou Nine Ring Fu Da Industrial Co., Ltd, Hangzhou, China). The exposure conditions used were those listed in the standard ASTM G154-12a (2014). Every 8 h cycle of simulated weathering consisted of 4 h of light irradiation at a black panel temperature of 60 °C and 4 h of condensation at a black panel temperature of 50 °C, in order to simulate day time and night time conditions, respectively. The procedure was interrupted after 24 h, 72 h, 120 h, 168 h, and 216 h of treatment, and the color was measured. To guarantee the accuracy of the data, the irradiated specimens were placed at room temperature for 1 d before each measurement.

Statistical analysis

Analysis of variance was performed on the experimental data using the software SPSS (Version 21.0, IBM, New York, USA). The curves were drawn using OriginLab OriginPro 2016 (Version 2016 SR0 b9.3.226, OriginLab Corporation, Northampton, USA).

Characterization

Scanning electron microscopy (SEM) analysis

The structures of the OBFRC samples were observed using an SEM system (S-3400N, Hitachi, Tokyo, Japan), which was operated at an accelerating voltage of 15 kV. Samples A_o, B_o, C_o, and D_o were treated with purified water at 85 °C for 6 h, 7 h, 8 h, and 9 h, respectively, and 50-μm cross-sections of the OBFRCs were obtained using a slicer (HM 430, Microm, Walldorf, Germany). This was done to cause the samples to expand, which allowed for better observations. Prior to the SEM imaging process, the cross-sections were coated with gold/palladium in a vacuum sputter coater.

Physical and mechanical properties of OBFRCs

Blocks with dimensions of 300 mm × 25 mm × 18 mm and 120 mm × 40 mm × 18 mm (longitudinal × radial × tangential) were cut from the pristine samples of the four different densities. Five samples were randomly selected, and the MOR and MOE values were measured. The HS measurements were performed six times on each sample type using standard GB/T 20241-2006 (2006). The static bending tests were performed using the standard GB/T 17657-2013 (2013) system in the three-point bending mode. More than 15 tests were performed for each sample type. The span used was 90 mm, and the loading rate was 5 mm/min. The MOR and MOE values were measured parallel to the face grains.

To evaluate moisture tolerance, four samples corresponding to each density were conditioned at 20 ± 2 °C and RH of $65 \pm 5\%$ until their masses became constant. Their weights and dimensions were measured. They were then soaked in 0.5% fungicide (provided by Beijing Forestry University) for 20 min and placed outdoors in Hangzhou city (120.2°E, 30.3°N) for 60 days from November 9, 2016 to January 9, 2017, when their weights and dimensions were measured again. All test samples were then placed in deionized water at 63 °C. The weights and dimensions of the pristine and naturally weathered samples were tested after 12, 24, 48, and 96 h of immersion. The WAR and VSE values were calculated as the markers of dimensional stability using Eqs. 2 and 3,

$$WAR_n(\%) = \frac{W_n - W_i}{W_i} \times 100\% \quad (2)$$

$$VSE_n(\%) = \frac{V_n - V_i}{V_i} \times 100\% \quad (3)$$

where W_n is the weight of the sample in question after being immersed for n hours, W_i is the original weight of the sample, V_n is the volume of the sample after being immersed for n hours, and V_i is original volume of the sample.

Color measurements

Three color measurements were performed on each sample using a Konica Minolta CR-10 system (Tokyo, Japan). The measurements were made in accordance with the ASTM E134706 standard (2007). For every specimen, the color changes induced during weathering were measured at the same location, in accordance with the Commission Internationale de l'Éclairage (CIE) Lab parameters, namely, the L^* axis represents the lightness, while a^* (redness) and b^* (yellowness) are the chromaticity coordinates. The differences in the chromaticity parameters (ΔL^* , Δa^* , and Δb^*) of the specimens before and after exposure were calculated using Eqs. 4 to 6,

$$\Delta L^* = L_t^* - L_o^* \quad (4)$$

$$\Delta a^* = a_t^* - a_o^* \quad (5)$$

$$\Delta b^* = b_t^* - b_o^* \quad (6)$$

where the subscripts o and t denote the values of the parameters before and after exposure for t hours, respectively. The total difference in the specimen color (ΔE^*) before and after exposure was calculated using Eq. 7. Color data was collected from three specimens, and the measurements were performed at three different locations for each specimen and the average data was recorded.

$$\Delta E^* = \sqrt{(\Delta L^*)^2 + (\Delta a^*)^2 + (\Delta b^*)^2} \quad (7)$$

Glossiness measurements

The glossiness was determined with the ASTM D523 standard (2014) by using a 60° universal gloss meter, which directed light at an incidence angle of 60° onto the sample surface and simultaneously measured the amount of light reflected. The results were based on a specular gloss value of 100, which corresponded to identical illumination and viewing conditions for a highly polished, plain black glass surface. The difference in the glossiness values was represented as the gloss retention rate (ΔG), which was calculated using the following formula,

$$\Delta G = \frac{(G_t - G_o)}{G_o} \times 100\% \quad (8)$$

where the subscripts o and t denote the values before and after the exposure, respectively, of the specimen in question to the weathering conditions for t hours. Five replicate measurements were performed on each sample surface.

Surface roughness measurements

A JB-4C precision roughness tester (Shanghai Taiming Optical Instrument Co., Ltd., Shanghai, China) was used to measure the surface roughness. The cut-off length was 2.5 mm, the sampling length was 12.5 mm, and the detector tip radius was 5 mm. Two replicates were used for each sample type. The relative roughness, R'_a , which is the ratio of the mean arithmetic deviation in R_a before and after UV irradiation (Kamdem and Grelier 2002), was calculated to evaluate the surface roughness of the pristine and weathered specimens using Eq. 9 in accordance with the GB/T 3505-2000 standard (2000),

$$R'_a = \frac{R_{at}}{R_{ao}} \quad (9)$$

where R_{at} is the roughness of the OBFRC sample in equation after weathering and R_{ao} is the roughness before weathering.

Contact angle measurements

Specimens were cut into slides with dimensions of 150 mm × 25 mm × 18 mm. Prior to the contact angle (CA) measurements, the board surface of the pristine control samples was sanded. Papers with grits of 100# and 180# were used in sequence. The CAs of three reference liquids (Table 2) on the surfaces of the pristine samples and samples subjected to accelerated weathering for 216 h were measured by the sessile drop method using a contact angle analyser (DSA 100, Krüss, Hamburg, Germany). Each sample was tested in triplicate in the same zone. Data collection began as soon as it was confirmed that the test droplets had touched the sample surface, typically within 0 to 3 frames (1 frame ≈ 19.2 ms). The value measured during the first frame was the initial CA. The data were collected within 60 s from the start of the measurements.

Table 2. Information about Three Reference Liquids

Reference Liquids	Molecular Formula	Molecular mass	Supplier
Deionized Water	H ₂ O	18.01	Treated by SMART Series SNW Ultra-pure Water System (Heal Force Bio-Meditech Holdings Limited, Heal Force, Shanghai, China)
Formamide	HCONH ₂	45.04	Chengdu Kelong Chemical Reagent Co., Ltd., China
Diiodomethane	CH ₂ I ₂	267.84	Aladdin Industrial Corporation, China

Calculation of surface free energy (SFE)

The surface tension components of the test liquids are listed in Table 3. As described in Fombuena *et al.* (2013) and Wang *et al.* (2015), the SFE values of the samples of different densities were calculated using the Lifshitz-van der Waals acid-base approach (Van Oss *et al.* 1988). As suggested by Bryne and Walinder (2010), the SFE values of the samples were determined based on the initial contact angles of water (polar), formamide (polar), and diiodomethane (nonpolar) using Eqs. 10 to 12,

$$\gamma_S = \gamma_S^{LW} + \gamma_S^{AB} \quad (10)$$

$$\gamma_S^{AB} = 2\sqrt{\gamma_S^+ \gamma_S^-} \quad (11)$$

$$(1 + \cos \theta)\gamma_L = 2 \left(\sqrt{\gamma_S^{LW} \gamma_L^{LW}} + \sqrt{\gamma_S^+ \gamma_L^-} + \sqrt{\gamma_S^- \gamma_L^+} \right) \quad (12)$$

where γ_S is the surface free energy of the OBFRC sample in question (mJ/m²), γ_S^{LW} is the apolar (Lifshitz-van der Waals) component of the surface free energy of the OBFRC (mJ/m²), γ_S^{AB} is the polar (Lewis acid-base) component of the surface free energy (mJ/m²), γ_S^+ is the electron-accepting component of the acid-base components of the OBFRC (mJ/m²), γ_S^- is the electron-donating component of the acid-base components (mJ/m²), θ is the contact angle of the liquid on the OBFRC (degrees), γ_L^{LW} is the apolar component of the liquid surface free energy (mJ/m²), γ_L^+ is the electron-accepting component of the liquid acid-base components (mJ/m²), and γ_L^- is the electron-donating component of the liquid acid-base components (mJ/m²).

Table 3. Surface Tension Components of Liquids used for Contact Angle Measurements

Reference Liquids	γ_L (mJ/m ²)	γ_L^{LW} (mJ/m ²)	γ_L^+ (mJ/m ²)	γ_L^- (mJ/m ²)
Water	72.80	21.80	25.50	25.50
Formamide	58.00	39.00	2.28	39.60
Diiodomethane	50.80	50.80	0.00	0.00

RESULTS AND DISCUSSION

SEM Analysis

Figure 2 shows cross-sectional SEM micrographs of the OBFRC samples, taken after the hot compression of the samples and after the expansion of the samples *via* water immersion. The vascular bundle, ground tissue cells, cell gap, and axial parenchyma were observed clearly in the cross-sections. Figure 2a shows that most of the pores of the basic tissue cells and the secondary xylem vessels were nearly circular and retained their original shape. A slight deformation of the oval pores was observed in the SEM micrograph of the sample with a density of 1.00 g/cm³. The cells of the sample with a density of 1.11 g/cm³ showed a greater degree of distortion (Fig. 2c, d). Similar changes were also observed in the intercellular spaces. Thus, it can be inferred that the deformation rate of the OBFRCs is positively correlated with the sample density. This phenomenon is attributable to the pressure applied to achieve the different densities as well as the large cell lumen and thin walls of the major cellular elements (*e.g.*, vascular bundles, ground tissue, and axial parenchyma). The high pressure and temperature during the hot-pressing process readily reshaped the tissue by decreasing the space of the cell lumen, resulting in more cell wall material per unit volume and thus increased density.

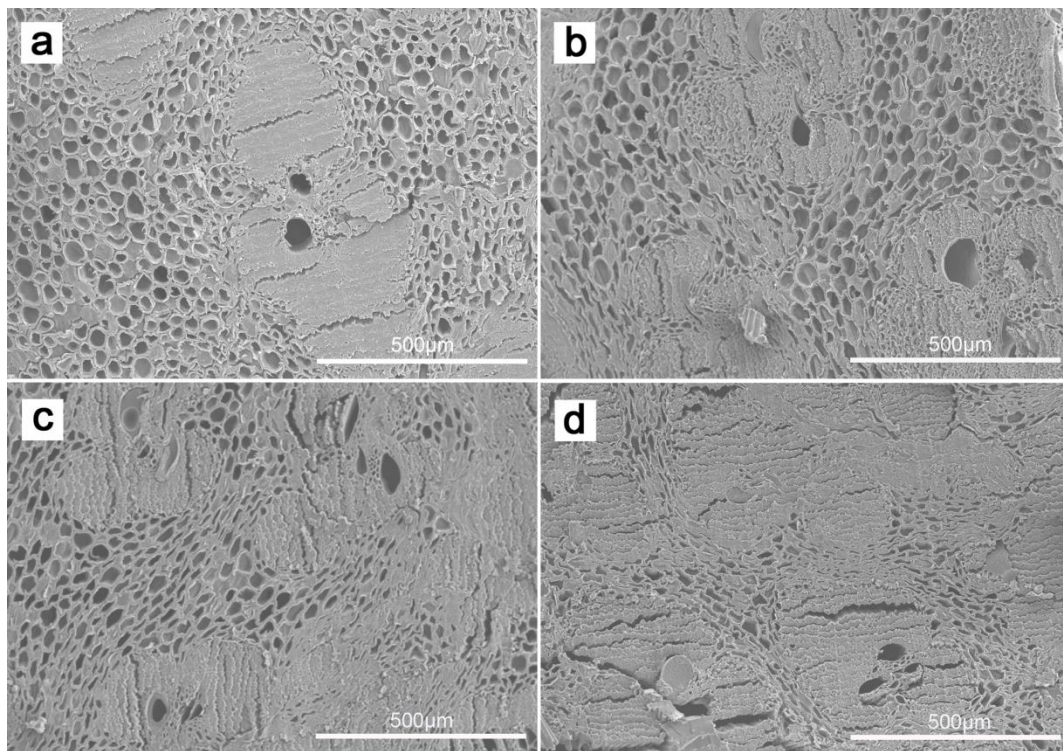


Fig. 2. SEM images of pristine OBFRC samples: (a) A₀, density of 0.91 g/cm³; (b) B₀, density of 1.00 g/cm³; (c) C₀, density of 1.11 g/cm³; and (d) D₀, density of 1.21 g/cm³

Physical and Mechanical Properties

Bending strength

Photodegradation is a phenomenon that occurred only on the surface (<200 μm) (Evans *et al.* 2005). It has a slight effect on the mechanical properties of materials

(Cogulet *et al.* 2016) owing to the limited penetration of wood by light (Kataoka *et al.* 2005). Thus, the MOE, MOR, and HS values of the samples after weathering were not tested. The average MOR and MOE values of the OBFRC samples of four different densities as well as the standard deviations (SD) are shown in Fig. 3. The bending properties of the composites are positively correlated with the density. The analysis of variance results indicate that the density has obvious influence on the bending performance. The MOR and MOE values increased with the density from 132.53 MPa (sample A_o, 0.90 g/cm³) to 170.51 MPa (sample D_o, 1.20 g/cm³) and from 11.13609 GPa (sample A_o, 0.90 g/cm³) to 13.10105 GPa (sample D_o, 1.20 g/cm³).

Cracks were found in the OBFMs on the inner and outer cylinder walls of the bamboo tubes and, in particular, linear ones with an average depth of 800 μm and width of 30 to 300 μm, contribute to the strength of OBFRCs by allowing adhesives to penetrate and the internal stress of the inner cylinder walls to be released (Yu *et al.* 2014). These results can be explained by the fact that higher-density composites have a greater amount of polymers per unit volume, due to there being a greater contact between plies after the hot-pressing process, in contrast to lower-density boards (Zhu and Yu 2010; Jeang-Kwan and Jong-Bum 2009). Notably, due to the heterogeneity of permeability in different parts of bamboo, the test specimens demonstrated most of the bond failure at the interfaces between the OBFMs during the bending tests. This observation confirmed that the higher-density composites exhibited greater internal stress (Jeang-Kwan and Jong-Bum 2009).

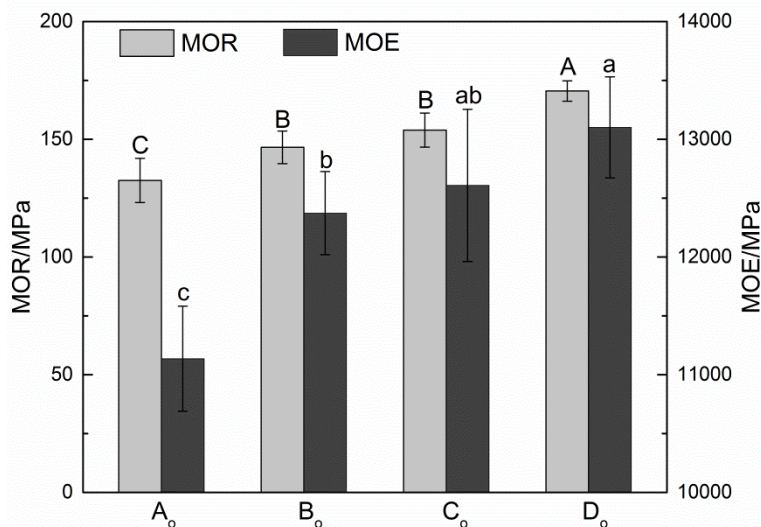


Fig. 3. Bending properties of pristine OBFRC samples. Different letters within a column indicate significant differences as determined by Duncan's multiple range test ($p < 0.05$, $N = 5$).

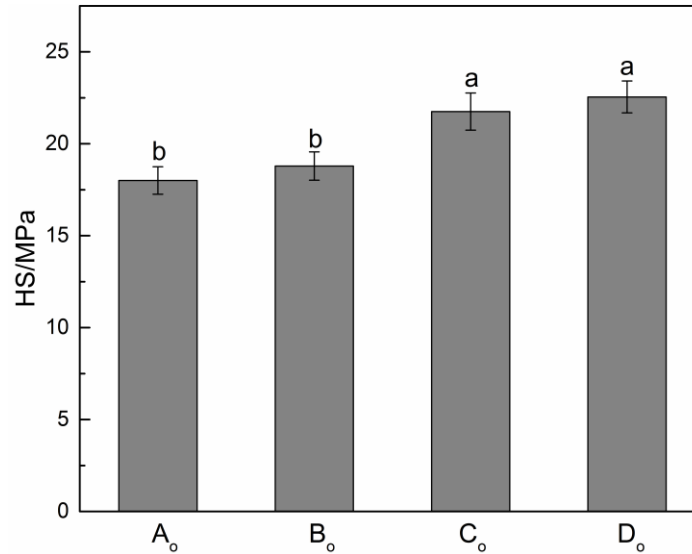


Fig. 4. HS strength of pristine OBFRC samples. Different lower-case letters within a column indicate significant differences as determined by Duncan's multiple range test ($p < 0.05$, $N = 6$)

Horizontal shear strength

The horizontal shear strength is primarily indicative of the performance of the bonding between the various layers under external loading, which is one of the safety indexes of the material. Figure 4 shows the horizontal shear (HS) strength of the OBFRC samples of four different densities. The results of the HS tests were similar to those of the bending strength tests. The HS increased from 18.0 for the sample with a density of 0.90 g/cm^3 to 22.5 MPa for the sample with a density of 1.17 g/cm^3 , and all HS values were much higher than those stated in the GB/T 30364-2013 standard (2013) for outdoor floors. In the present study, all samples failed because of their interlaminar shear failure. The results of the HS tests further confirmed that increasing the density has a positive effect on the mechanical properties related to material strength, primarily because of resin impregnation, increased fiber aggregation, and greater adhesive contact between the fibrotic veneers per unit volume. Considering the matrix material, processing cost, and mechanical performance, it can be concluded that a density of 1.1 g/cm^3 is the most suitable for the industrial production of OBFRCs.

Water absorption

A longer service life under outdoor conditions requires OBFRCs to retain their mechanical properties and dimensional stability and to withstand diverse natural environments, which necessitate a high water resistance. The changes in the moisture content of composites in response to rain, snow, and water vapor are primarily determined by the dimensional properties of the composites. Figure 5 shows the effects of the density of the OBFRCs fabricated in this study on their water absorption properties.

As observed in compressed weeping willow (*Salix babylonica*) wood panels (Li *et al.* 2017), the WAR of the OBFRC samples decreased with an increase in the density (Fig. 5a), while the VSE showed the opposite trend (Fig. 5b). The WAR values of the pristine samples and naturally weathered samples with a density of 1.20 g/cm^3 were approximately half of the samples with a density of 0.90 g/cm^3 after being immersed in water for 96 h at $63 \text{ }^\circ\text{C}$, while the VSE values of the former were 1.9 and 2.0 times higher, respectively. In high-density composites with a compact internal structure, the

pores are smaller and more dotted and/or linear cracks are blocked by adhesive (Yu *et al.* 2014) because the water cannot easily penetrate the material. The thickness swelling rate (TSR) of wood/bamboo-based reconstituted composites makes the largest contribution to the VSE (Zhu *et al.* 2015; Zhu and Yu 2010; Bao *et al.* 2016). The hot-pressing process and the compression springback of the composite together increase the TSR (Zhang *et al.* 2016). The fabrication of the high-density OBFRCs requires higher pressures because the internal stresses in the composites are higher. As a result, their compression springback becomes the main factor affecting the TSR. However, the low-density OBFRCs have more pores for absorbing water during immersion (Fig. 2). Therefore, a higher density resulted in a greater VSE in the case of the OBFRCs. The WAR and VSE values of the naturally weathered samples were lower than those of the pristine samples by an average of 4.20% and 0.48%, respectively (Fig. 5).

Results indicate that natural weathering treatment improves the water resistance of the samples. The surface delignification of the bamboo-based materials began after outdoor weathering for 1 day, with the materials undergoing almost complete delignification after exposure for 1 week (Pandey and Pitman 2002). After the loss of lignin from the intercellular layer, cross-sectional images of the irradiated samples revealed that noticeable damage had occurred to the fiber walls, which was not conducive to the diffusion of water into the cells (Wang and Ren 2009). In addition, the number of free hydroxyl groups in the weathered samples for binding with water molecules to form new hydrogen bonds was reduced and the surface bamboo crystallinity was increased. These factors resulted in a decrease in the hygroscopicity of the OBFRCs.

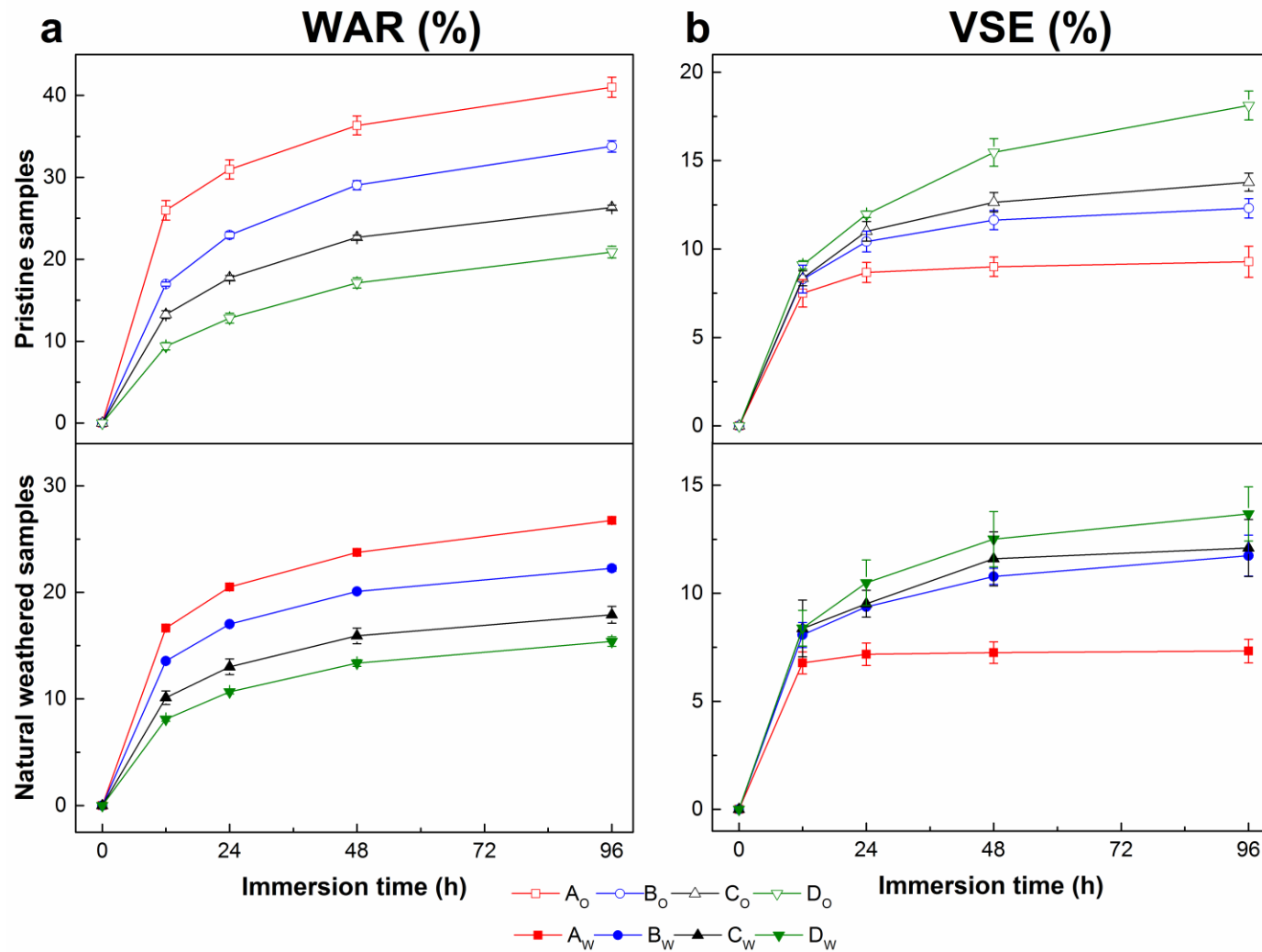


Fig. 5. (a) Water absorption rate (WAR) and (b) volume swelling efficiency (VSE) values of pristine and naturally weathered OBFR samples of different densities

Surface Properties

OBFRCs are susceptible to surface degradation during outdoor exposure, with the exposure primarily resulting in color changes, the disappearance of gloss, surface roughening, and a decrease in the wettability over time (Gindl *et al.* 2004; Wang and Ren 2008, 2009; Anwar *et al.* 2011; Zhu *et al.* 2015).

Color changes during accelerated weathering

The above-mentioned color changes are related to chemical changes such as lignin degradation and carboxyl formation (Qin and Yu 2009), which degrades the aesthetics of the material surface. The color changes in response to the UV irradiation of the surfaces of the OBFRCs with the different densities are shown in Fig. 6.

The value of ΔL^* during and after 216 h of exposure is shown in Fig. 6a. The ΔL^* value decreased with the irradiation time, indicating that the OBFRCs darkened with increased exposure (Temiz *et al.* 2005). The decrease in ΔL^* was reduced with an increase in the sample density, with the smallest ΔL^* value being observed for sample D_w (-7.04) after 216 h of exposure. Thus, a higher density helps prevent decreases in lightness upon UV exposure.

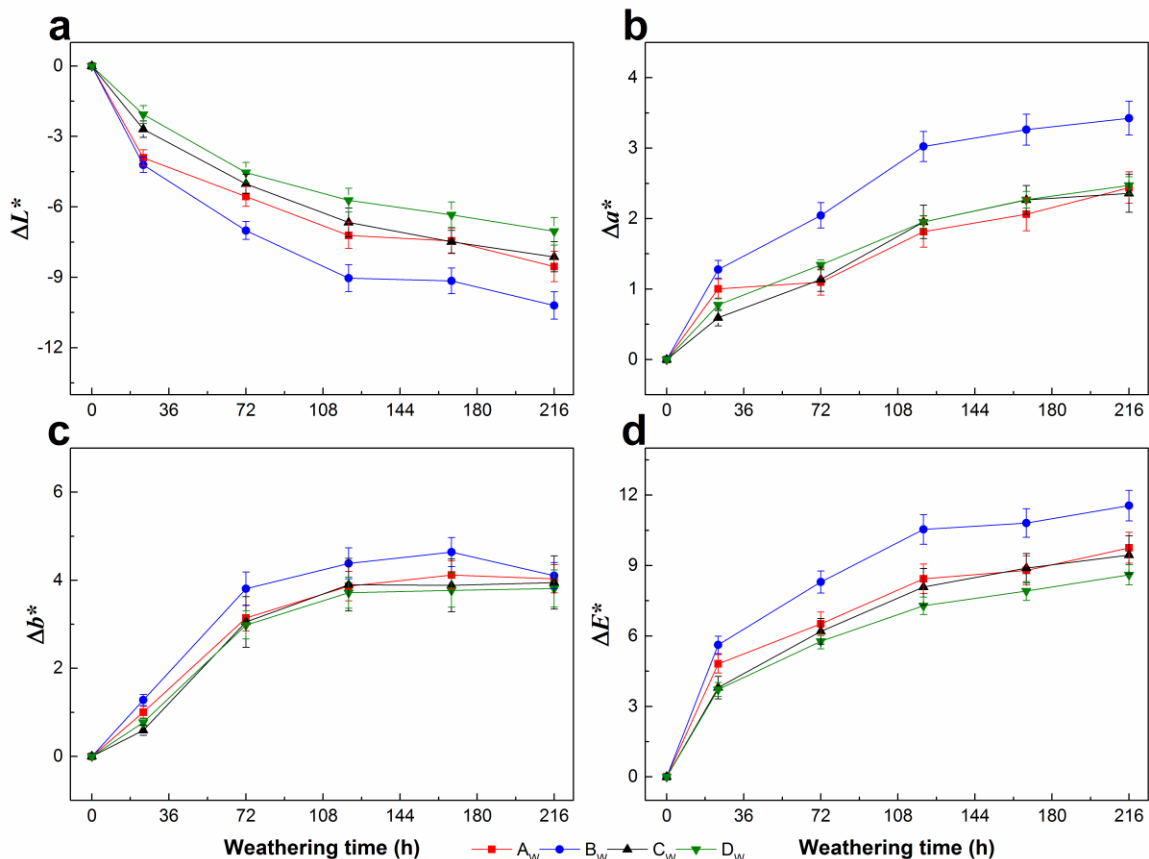


Fig. 6. (a) ΔL^* , (b) Δa^* , (c) Δb^* , and (d) ΔE^* values of OBFRCs with different densities as functions of duration of UV accelerated weathering

The changes in the parameters a^* and b^* of the OBFRCs are shown in Fig. 6b, and 6c. Both Δa^* and Δb^* increased with increasing of irradiation time. Sample B_w showed the largest value of Δa^* after 216 h of exposure. The changes in the case of the other samples were not significant. In the first 120 h of exposure, the differences in the Δb^* values were more pronounced and resulted in a slight yellowing effect. Sample B_w underwent yellowing to the greatest extent during the weathering process. Previous studies have shown that a quick change in color occurs in the rapid phase of the photochemical reaction (Arnold *et al.* 1991; Müller *et al.* 2003; Kishino and Nakano 2004; Baysal *et al.* 2014). This kind of reaction tends to reach a point of equilibrium because of the slow diffusion of oxygen and the free radicals (which are necessary for the reaction) from the material surface to its interior (Arnold *et al.* 1991). On the macroscale, this is reflected as a decrease in the rate of color change.

The ΔE^* value represents the overall difference in the color modulus or the color stability, which can be observed by the naked eye, when the value of ΔE^* is greater than 8. The ΔE^* values of the OBFRCs of different densities with different exposure times are compared in Fig. 6d.

In contrast to five wood species (*Picea abies*, *Pinus sylvestris*, *Larix decidua*, *Populus euramericana*, and *Robinia pseudoacacia*), the ΔE^* value of the OBFRCs increased rapidly to 10 to 15 in the first 50 h of exposure (Tolvaj and Faix 1995). Furthermore, sample B_w was 11.55 after 120 h of exposure, while the values of the other samples were between 6 and 8. These results suggest that the effects of weathering on the chemical composition of the OBFRCs were weaker than that on the composition of wood and that the former exhibited higher resistance to color change. Based on the ΔE^* values after exposure for 216 h, the color stability of the samples could be arranged in the following order: D_w (8.61) > C_w (9.45) > A_w (9.89) > B_w (11.55). Ignoring the nonhomogeneous nature of the OBFRCs, it can be concluded that higher-density materials will show greater color stability.

Wang and Ren (2008) obtained similar results after exposing *Phyllostachys pubescens* Mazel bamboo to artificial sunlight from a Xe lamp. Overall, these results indicate that bamboo and its products have a greater resistance to photoinduced discoloration than wood does (Zhu *et al.* 2015; Wang and Ren 2008).

The weathered samples showed decreased chroma and increased darkening as the duration of the exposure was increased. As the OBFRCs are nonhomogeneous materials, different samples exhibited different color changes. However, overall, a higher density resulted in greater chromic stability with an increase in the irradiation time.

Glossiness retention

The loss of glossiness was very rapid in the first 24 h of irradiation (Fig. 7). The minimum and maximum initial gloss values, which were 1.92 and 2.40, were exhibited by samples B_w and D_w, respectively.

For all samples, the glossiness was affected only slightly by the exposure time during the exposure period extending from 24 h to 168 h. The final gloss value of sample D_w was the highest, at 1.65, while sample C_w exhibited the lowest value, which was 1.27. All the samples showed only a small change in glossiness and this suggests that the OBFRCs retained their glossiness after weathering.

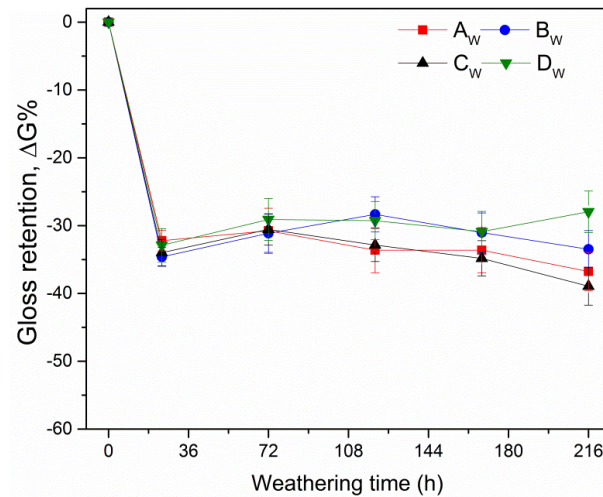


Fig. 7. Change in glossiness of OBFRC samples during artificial weathering

Roughness

The relative surface roughness (R'_a) values of the OBFRC samples of different densities after 216 h of exposure are shown in Fig. 8. The R'_a values ranged from 3.66 (for the sample with a density 0.9 g/cm³) to 4.94 (for the sample with a density 1.2 g/cm³). These values were remarkably higher than those of chemically modified wood (Kamdern and Grelier 2002), which indicates that the surface roughness of the OBFRCs increases sharply after weathering. The R'_a values of the samples with densities of 1.0 g/cm³ and 1.1 g/cm³ were approximately 4.04 and 4.10, respectively.

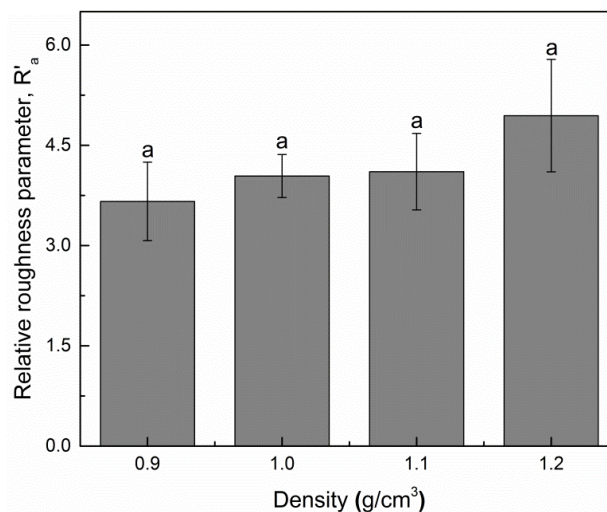


Fig. 8. Relative surface roughness versus density after 216 h of exposure

There are several reasons for the increase in the roughness after weathering. First, the pristine samples were sanded before the weathering treatment. For the weathered samples, the surface lignin underwent degradation during the outdoor exposure treatment, which resulted in the formation of a cellulose layer on the surface (Evan *et al.* 2005; Cogulet *et al.* 2016), as well as yellowing (Müller *et al.* 2003) (Fig. 6). In addition, cracks were formed in the cell walls (Wang and Ren 2009). Secondly, water accelerates the loss of the soluble lignin degradation products because the surface fibers loosen and are

directly exposed to UV radiation (Wang and Ren 2009). It is likely that moisture caused the unequal distribution of stress in the material which resulted in surface cracks. In addition, with an increase in the density, the R'_a value increased, which suggests that the density affects the changes induced in the surface roughness during the weathering process. However, variance analysis showed that the density had no significant effect on relative surface roughness.

Wettability

The contact angle and surface energy data of wood can be used to determine the wettability of wood with respect to various liquids, including coatings and glues. The density of composite materials has a significant effect on their wettability (Bao *et al.* 2016). Table 4 displays the initial CAs of different reference liquids on the surfaces of the OBFRC samples of different densities.

Table 4. Initial Contact Angles of Different Reference Liquids on OBFRC Surface

Samples		Water Contact Angle (°)	Formamide Contact Angle (°)	Diiodomethane Contact Angle (°)
Pristine Samples	A _o	62.78	48.03	38.99
	B _o	63.32	55.85	43.18
	C _o	65.08	61.59	45.29
	D _o	65.90	63.51	48.35
Weathered Samples	A _w	78.83	78.56	57.47
	B _w	81.49	81.61	56.22
	C _w	82.66	82.55	55.55
	D _w	87.41	82.98	51.19

The initial CAs for all the reference liquids at the same density level increased to different degrees after weathering, which suggests that the sample surface becomes more hydrophobic after weathering (Kalnins and Knaebe 1992). In the case of the polar liquids (water and formamide), the initial CAs on the pristine and weathered OBFRC samples are positively correlated with the density. This result is consistent with the changes in the CA of the nonpolar liquid (diiodomethane) with the density before weathering. However, the initial CA of diiodomethane on the surfaces of the weathered OBFRC samples was negatively correlated with the density. Figure 9 shows the dynamic CAs of the three different liquids as functions of time for the untreated OBFRC samples of different densities. A higher density resulted in a greater CA on the surfaces of the pristine OBFRC samples, which was true for all three liquids, and which is also the case with composites (Bao *et al.* 2016). After the weathering treatment, there were small differences in the CAs of water and formamide on the samples of different densities. Furthermore, the CA of diiodomethane showed a negative correlation with the density. This may be due to the differences in the interactions between the sample surfaces and the reference liquids, which had different chemical structures, as well as the degradation of the chemical components of bamboo. The weathering treatment accelerated the speed with which water spread on the OBFRC surface (Fig. 9a) but had almost no effect (Fig. 9b) on the spreading speed of formamide and slightly retarded the spreading of diiodomethane (Fig. 9c). These results indicate that the weathering process led to an increase in the hydrophobicity of the OBFRC samples, with the increase in the hydrophobicity being higher for higher densities.

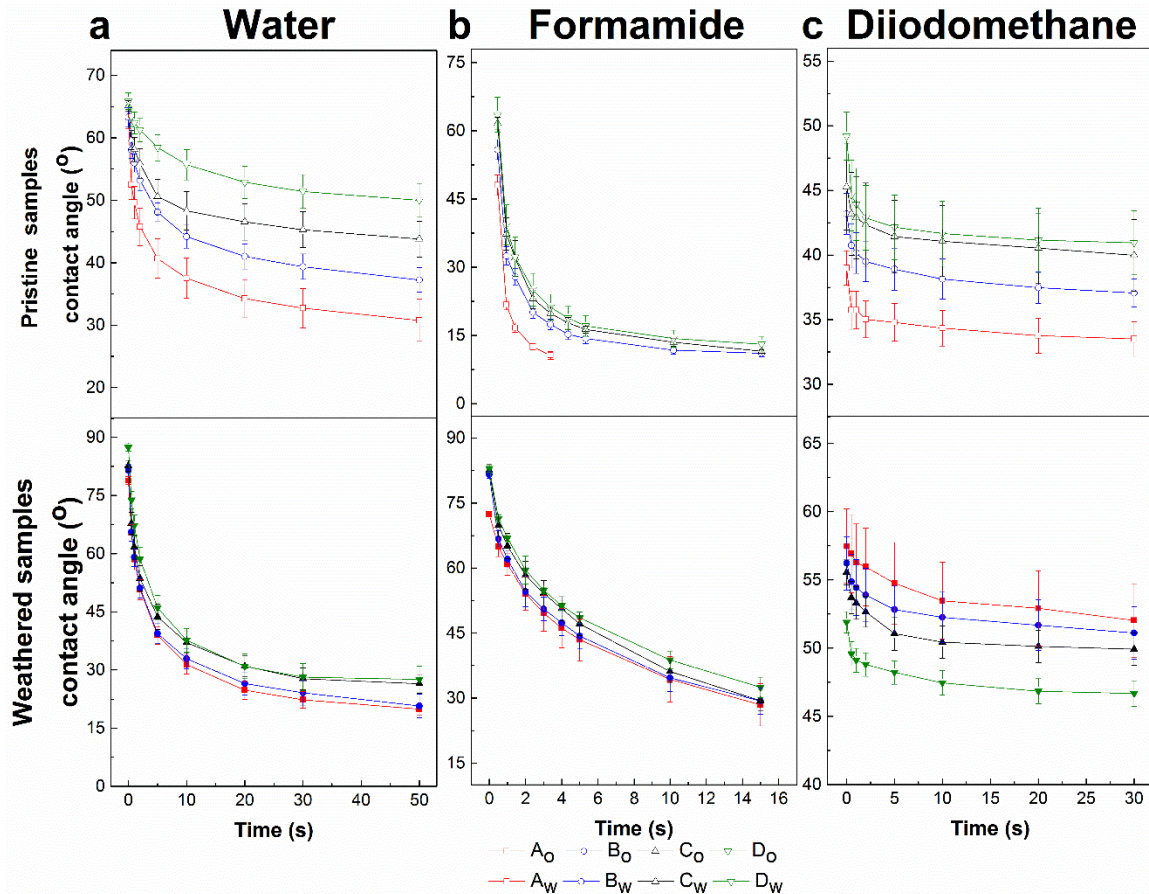


Fig. 9. Time dependence of dynamic contact angle of (a) water, (b) formamide, and (c) diiodomethane on pristine and weathered OBFRC surfaces

The surface free energy (γ_S) and its components (γ_S^{LW} , γ_S^{AB} , γ_S^+ and γ_S^-) of the pristine and weathered OBFRC samples of different densities were calculated (Table 5). The γ_S values of the pristine OBFRC samples ranged from 30 mJ/m² and 44 mJ/m², which were slightly lower than that of wood (Wang *et al.* 2015). As pine wood (*Pinus sylvestris* L.) (Shen *et al.* 1998), γ_S^{LW} was the major energy component for OBFRC as compared with γ_S^{AB} . Furthermore, it seemed that γ_S , γ_S^{LW} and γ_S^{AB} for the pristine samples depended on the density of OBFRC. These results reflected that the interactions were related to γ_S^{LW} (nonpolar interactions) and γ_S^{AB} (polar interactions), which both decreased with increased density. However, the weathered samples didn't conform to this correlation mainly due to the changes in the surface chemical composition. After the weathering treatment, the variation of γ_S^{LW} and γ_S^{AB} in OBFRCs of different densities were lower than in similar samples without weathering. However, the difference between γ_S^{LW} and γ_S^{AB} was greater than the pristine samples of the same density and the increase with greater density. Overall, weathering decreased the surface wettability. Although the surface free energy of the weathered samples was very low, the difference between the acid and base components was large, most likely due to the changes in the hydrophobicity after weathering.

Table 5. Surface Free Energies (γ_S) and Lifshitz-van der Waals (γ_S^{LW}), Lewis Acid-base (γ_S^{AB}), Electron Acceptor (γ_S^+), and Electron Donor (γ_S^-) Components of OBFRC Samples of Different Densities

Samples		γ_S (mJ/m ²)	γ_S^{LW} (mJ/m ²)	γ_S^{AB} (mJ/m ²)	γ_S^+ (mJ/m ²)	γ_S^- (mJ/m ²)
Pristine Samples	A _o	43.32	40.12	3.20	0.14	18.27
	B _o	37.16	37.98	-0.81	0.007	23.34
	C _o	32.00	36.85	-4.55	0.20	25.81
	D _o	30.50	35.19	-4.70	0.21	26.26
Weathered Samples	A _w	20.81	30.03	-9.22	1.03	20.71
	B _w	19.28	30.75	-11.47	1.67	19.70
	C _w	19.14	31.13	-12.00	1.90	18.92
	D _w	23.04	33.61	-10.57	2.12	13.18

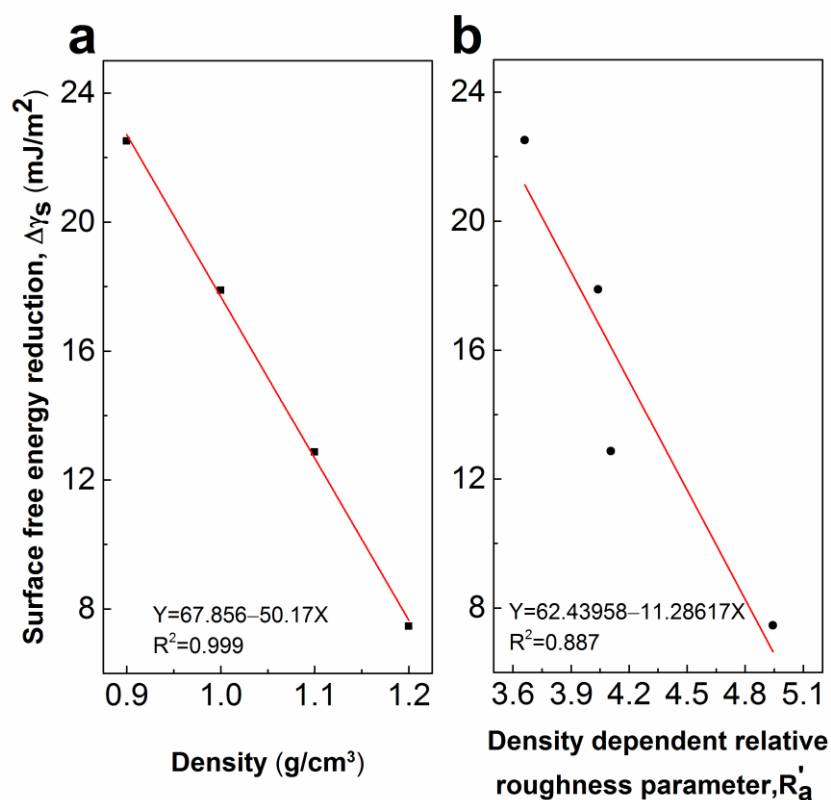


Fig. 10. (a) Decrease in surface free energy of OBFRC versus density and (b) density-dependent relative roughness of OBFRCs after 216 h of UV irradiation

Figure 10 shows the correlations between the sample density or density-dependent relative roughness (R_a') and the surface free energy reduction ($\Delta\gamma_S$) for the OBFRC samples of the same density due to weathering (Fig. 10b). The OBFRC was made from carbonized OBFMs and subsequently exposed to ultraviolet radiation. Hemicellulose, amorphous cellulose and lignin could be degraded by different degrees during the heat treatment and weathering, respectively (Esteves and Pereira 2009; Wang and Ren 2009; Zhang *et al.* 2013; Yu *et al.* 2015). The decrease in the hydrophilic components of the OBFRC resulted in an increase in the surface hydrophobicity. Figure 10a shows a linear relationship (slope is -50.17) between the sample density and $\Delta\gamma_S$ for the densities of 0.9

g/cm^3 to 1.2 g/cm^3 , indicating that the high-density OBFRC samples showed high resistance to decreases in their wettability during the weathering process. Moreover, this result can be used to reliably predict the change in the wettability of OBFRCs with changes in their density under outdoor conditions. A linear relationship (slope of -11.28617) was also observed between R'_a and $\Delta\gamma_s$ (Fig. 10b). After the weathering treatment, the surface roughness and the wettability retention increased with the increase of density. The rougher and more hydrophobic surface caused the losing performance of finishes, coating ability and glueability. R'_a increased with the greater density, but $\Delta\gamma_s$ appeared to represent an opposite trend (Fig. 10b). Surface sanding could eliminate the differences in surface weathering properties due to the various densities. Therefore, the density-based surface sanding is an advantageous processing step prior to the finish application (Richter *et al.* 1995). Reasonable surface sanding before coating can maintain the performance of OBFRC for construction and decoration purposes, so as to improve its competitiveness of outdoor application.

CONCLUSIONS

1. With an increase in density, the degree of compression of the OBFRCs, the VSE, and the surface CA of the reference liquids increased, and the physical and mechanical properties of the OBFRCs improved. In contrast, the surface free energy and water absorption rate decreased gradually.
2. After artificial accelerated weathering and natural weathering (water absorption) treatments, the surface contact angle, surface roughness, and dimensional stability increased while the surface glossiness, water absorption, and surface free energy decreased.
3. The surfaces of the OBFRCs became darker and faded and turned red and yellow under accelerated weathering. Furthermore, a higher density meant improved color stability, thus confirming that the density of OBFRCs is one of the most important factors affecting their outdoor performance.
4. Density-increasing treatments are advantageous because they enhance the physical and mechanical properties of OBFRCs and prevent decreases in their wettability and color over certain durations of accelerated weathering. However, they also decrease the dimensional stability, while increasing the relative roughness and production cost. Thus, based on the results of this study, a density of 1.1 g/cm^3 is the most appropriate for OBFRCs that are produced for general applications.

ACKNOWLEDGEMENTS

This work was supported by the Fundamental Research Funds for the Central Non-profit Research Institution of CAF (CAFYBB2017ZX003-12) and the Science and Technology Planned Projects of Zhejiang Province under Grant (2016F50006; 2015F50054).

REFERENCES CITED

- Anwar, U. M. K., Hiziroglu, S., Hamdan, H., and Abd. Latif, M. (2011). "Effect of outdoor exposure on some properties of resin-treated plybamboo," *Industrial Crops and Products* 33(1), 140-145. DOI: 10.1016/j.indcrop.2010.09.014
- Arnold, M., Sell, J., and Feist, W. C. (1991). "Wood weathering in fluorescent ultraviolet and xenon arc chambers," *Forest Products Journal* 41(2), 40-44.
- ASTM D523 (2014). "Standard test method for specular gloss," ASTM International, West Conshohocken, PA. DOI: 10.1520/C0231
- ASTM E1347-06 (2007). "Standard test method for color and color-difference measurement by tristimulus," ASTM International, West Conshohocken, PA. DOI: 10.1520/E1347-06.
- ASTM G154-12a (2014). "Standard practice for operating fluorescent ultraviolet (UV) Lamp apparatus for exposure of nonmetallic materials," ASTM International, West Conshohocken, PA. DOI: 10.1520/G0154-12a.2
- Bao, M., Huang, X., Zhang, Y., Yu, W., and Yu, Y. (2016). "Effect of density on the hygroscopicity and surface characteristics of hybrid poplar compreg," *Journal of Wood Science* 62(5), 1-11. DOI: 10.1007/s10086-016-1573-4
- Baysal, E., Dizman Tomak, E., Ozbey, M., and Altin, E. (2014). "Surface properties of impregnated and varnished Scots pine wood after accelerated weathering," *Coloration Technology* 130(2), 140-146. DOI: 10.1111/cote.12070
- Beckers, E., de Meijer, M., Militz, H., and Stevens, M. (1998). "Performance of finishes on wood that is chemically modified by acetylation," *Journal of Coatings Technology* 70(3), 59-67. DOI: 10.1007/BF02697812
- Bryne, L. E., and Wälinder, M. E. P. (2010). "Ageing of modified wood. Part 1: Wetting properties of acetylated, furfurylated, and thermally modified wood," *Holzforschung* 64(3), 295-304. DOI: 10.1515/HF.2010.040
- Chaochanchaikul, K., Rosarpitak, V., and Sombatsompop, N. (2013). "Photodegradation profiles of PVC compound and wood/PVC composites under UV weathering," *Express Polymer Letters* 7(2), 146-160. DOI: 10.3144/expresspolymlett.2013.14
- Cogulet, A., Blanchet, P., and Landry, V. (2016). "Wood degradation under UV irradiation: A lignin characterization," *Journal of Photochemistry and Photobiology B: Biology* 158, 184-191. DOI: 10.1016/j.jphotobiol.2016.02.030
- Cristea, M. V., Riedl, B., and Blanchet, P. (2010). "Enhancing the performance of exterior waterborne coatings for wood by inorganic nanosized UV absorbers," *Progress in Organic Coatings* 69(4), 432-441. DOI: 10.1016/j.porgcoat.2010.08.006
- Esteves, B. M., and Pereira, H. M. (2009). "Wood modification by heat treatment: A review," *BioResources*, 4(1), 370-404. DOI: 10.15376/biores.4.1.370-404
- Evans, P., Chowdhury, M. J., Mathews, B., Schmalzl, K., Ayer, S., Kiguchi, M., Kataoka, Y. (2005). "Chapter 14: Weathering and surface protection of wood," in: *Handbook of Environmental Degradation of Materials*, M. Kutz (ed.), William Andrew, Norwich, NY, pp. 277-297.
- Fombuena, V., Balart, J., Boronat, T., Sánchez-Nácher, L., and Garcia-Sanoguera, D. (2013). "Improving mechanical performance of thermoplastic adhesion joints by atmospheric plasma," *Materials and Design* 47, 49-56. DOI: 10.1016/j.matdes.2012.11.031
- GB/T 17657-2013 (2013). "Test methods of evaluating the properties of wood-based panels and surface decorated wood-based panels," National Organization for

- Standardization, China.
- GB/T 20241-2006 (2006). "Laminated veneer lumber," National Organization for Standardization, China.
- GB/T 30364-2013 (2013). "Bamboo scrimber flooring," National Organization for Standardization, China.
- GB/T 3505-2000 (2000). "Geometrical product specifications (GPS)-surface texture:profile method-terms,definitions and surface texture parameters." National Organization for Standardization, China.
- George, B., Suttie, E., Merlin, A., and Deglise, X. (2005). "Photodegradation and photostabilisation of wood - The state of the art," *Polymer Degradation and Stability* 88(2), 268-274. DOI: 10.1016/j.polymdegradstab.2004.10.018
- Gindl, M., Reiterer, A., Sinn, G., and Stanzl-Tschegg, S. E. (2004). "Effects of surface ageing on wettability, surface chemistry, and adhesion of wood," *Holz als Roh- und Werkstoff* 62(4), 273-280. DOI: 10.1007/s00107-004-0471-4
- Hayoz, P., Peter, W., and Rogez, D. (2003). "A new innovative stabilization method for the protection of natural wood," *Progress in Organic Coatings* 48(2-4), 297-309. DOI: 10.1016/S0300-9440(03)00102-4
- Horn, B. A., Qiu, J., Owen, N. L., and Feist, W. C. (1994). "FT-IR studies of weathering effects in western redcedar and southern pine," *Applied Spectroscopy Reviews* 48(6), 662-668. DOI: Doi 10.1366/000370294774369072
- Jeang-Kwan, R., and Jong-Bum, R. (2009). "Effect of moisture content and density on the mechanical properties of veneer-bamboo zephyr composites," *Forest Products Journal* 59(3), 75-78.
- Kamdem, D. P., and Grelier, S. (2002). "Surface roughness and color change of copper-amine treated red maple (*Acer rubrum*) exposed to artificial ultraviolet light," *Holzforschung* 56(5), 473-478. DOI: 10.1515/HF.2002.073
- Kataoka, Y., Kiguchi, M., Fujiwara, T., and Evans, P. D. (2005). "The effects of within-species and between-species variation in wood density on the photodegradation depth profiles of sugi (*Cryptomeria japonica*) and hinoki (*Chamaecyparis obtusa*)," *Journal of Wood Science* 51(5), 531-536. DOI: 10.1007/s10086-004-0685-4
- Kishino, M., and Nakano, T. (2004). "Artificial weathering of tropical woods. Part 2: Color change," *Holzforschung* 58(5), 558-565. DOI: 10.1515/HF.2004.085
- Lesar, B., Pavlič, M., Petrič, M., Škapin, A. S., and Humar, M. (2011). "Wax treatment of wood slows photodegradation," *Polymer Degradation and Stability* 96(7), 1271-1278. DOI: 10.1016/j.polymdegradstab.2011.04.006
- Li, N., Chen, Y., Bao, Y., Zhang, Z., Wu, Z., and Chen, Z. (2015). "Evaluation of UV-permeability and photo-oxidisability of organic ultraviolet radiation-absorbing coatings," *Applied Surface Science* 332, 186-191. DOI: 10.1016/j.apsusc.2015.01.112
- Li, N., Bao, M., Chen, Y., Zhang, Y., Bao, Y., and Yu, W. (2017). "Influence of density on properties of compressed weeping willow (*Salix babylonica*) wood panels," *Forest Products Journal* 67(1/2), 44-49.
- Müller, U., Rätzsch, M., Schwanninger, M., Steiner, M., and Zöbl, H. (2003). "Yellowing and IR-changes of spruce wood as result of UV-irradiation," *Journal of Photochemistry and Photobiology B: Biology* 69(2), 97-105. DOI: 10.1016/S1011-1344(02)00412-8
- Van Oss, C. J., Chaudhury, M. K., and Good, R. J. (1988). "Interfacial Lifshitz-van der Waals and polar interactions in macroscopic systems," *Chemical Reviews* 88(6), 927-941. DOI: 10.1021/cr00088a006

- Pandey, K. K. (2005). "Study of the effect of photo-irradiation on the surface chemistry of wood," *Polymer Degradation and Stability* 90(1), 9-20. DOI: 10.1016/j.polymdegradstab.2005.02.009
- Pandey, K. K., and Pitman, A. J. (2002). "Weathering characteristics of modified rubberwood (*Hevea brasiliensis*)," *Journal of Applied Polymer Science* 85(3), 622-631. DOI: 10.1002/app.10667
- Qin, L., and Yu, W. J. (2009). "Research on surface color, properties of thermo-treated reconstituted bamboo lumber after artificial weathering test," *Advanced Materials Research* 79–82, 1395-1398. DOI: 10.4028/www.scientific.net/AMR.79-82.1395
- Richter, K., Feist, W. C., and Knaebe, M. T. (1995). "The effect of surface roughness on the performance of finishes. 1. Roughness characterization and stain performance," *Forest Products Journal*, 45(1), 91-97.
- Shen, Q., Nylund, J., and Rosenholm, J. B. (1998). "Estimation of the surface energy and acid-base properties of wood by means of wetting method," *Holzforschung*, 52(5), 521–529. DOI: 10.1515/hfsg.1998.52.5.521
- Srinivas, K., and Pandey, K. K. (2012). "Photodegradation of thermally modified wood," *Journal of Photochemistry and Photobiology B: Biology* 117, 140-145. DOI: 10.1016/j.jphotobiol.2012.09.013
- Temiz, A., Yildiz, U. C., Aydin, I., Eikenes, M., Alfredsen, G., and Çolakoglu, G. (2005). "Surface roughness and color characteristics of wood treated with preservatives after accelerated weathering test," *Applied Surface Science* 250(1–4), 35-42. DOI: 10.1016/j.apsusc.2004.12.019
- Tolvaj, L., Nemeth, R., Pasztory, Z., Bejo, L., and Takats, P. (2014). "Colour stability of thermally modified wood during short-term photodegradation," *BioResources* 9(4), 6644-6651. DOI: 10.15376/biores.9.4.6644-6651
- Tolvaj, L., Persze, L., and Albert, L. (2011). "Thermal degradation of wood during photodegradation," *Journal of Photochemistry and Photobiology B: Biology* 105(1), 90-93. DOI: 10.1016/j.jphotobiol.2011.07.005
- Tomak, E. D., Topaloglu, E., Ay, N., and Yildiz, U. C. (2012). "Effect of accelerated aging on some physical and mechanical properties of bamboo," *Wood Science and Technology* 46(5), 905-918. DOI: 10.1007/s00226-011-0454-7
- Shangguan, W., Gong, Y., Zhao, R., and Ren., H. (2016). "Effects of heat treatment on the properties of bamboo fiber/polypropylene composites," *Fibers and Polymers* Springer Japan, 14(11), 1894-1898. DOI: 10.1007/s12221-013-1894-5
- Wang, W., Zhu, Y., Cao, J., and Guo, X. (2015). "Thermal modification of Southern pine combined with wax emulsion preimpregnation: Effect on hydrophobicity and dimensional stability," *Holzforschung* 69(4), 405-413. DOI: 10.1515/hf-2014-0106
- Wang, X. Q., and Ren, H. Q. (2009). "Surface deterioration of moso bamboo (*Phyllostachys pubescens*) induced by exposure to artificial sunlight," *Journal of Wood Science* 55(1), 47-52. DOI: 10.1007/s10086-008-0994-0
- Wang, X., and Ren, H. (2008). "Comparative study of the photo-discoloration of moso bamboo (*Phyllostachys pubescens* Mazel) and two wood species," *Applied Surface Science* 254(21), 7029-7034. DOI: 10.1016/j.apsusc.2008.05.121
- Weichelt, F., Beyer, M., Emmler, R., Flyunt, R., Beyer, E., and Buchmeiser, M. (2011). "Zinc oxide based coatings for the UV-protection of wood for outdoor applications," *Macromolecular Symposia* 301(1), 23-30.

- Yu, H., Yu, W., Yang, L., Fang, C., and Xu, M. (2015). "Surface discoloration analysis and lignin degradation fragments identification of UV-irradiated moso bamboo (*Phyllostachys pubescens* Mazel)," *BioResources* 10, 1617-1626.
- Yang, T., Chang, F., Lin, C., and Chang, F. (2016). "Effects of temperature and duration of heat treatment on the physical, surface, and mechanical properties of Japanese cedar wood," *BioResources* 11, 3947-3963. DOI: 10.15376/biores.11.2.3947-3963
- Yu, Y., Huang, X., and Yu, W. (2014). "A novel process to improve yield and mechanical performance of bamboo fiber reinforced composite via mechanical treatments," *Composites Part B: Engineering* 56, 48-53. DOI: 10.1016/j.compositesb.2013.08.007
- Zhang, Y. M., Yu, Y. L., and Yu, W. J. (2013). "Effect of thermal treatment on the physical and mechanical properties of phyllostachys pubescens bamboo," *European Journal of Wood and Wood Products*, 71(1), 61–67. DOI: 10.1007/s00107-012-0643-6
- Zhang, Y., Zhang, Y., and Yu, W. (2016). "Effect of density on light-soft wood scrimber properties," *China Wood-based Panels* 04, 10-13.
- Zhu, J., Yang, D., Geng, J., and Jiang, Z. (2008). "Synthesis and characterization of bamboo-like CdS/TiO₂ nanotubes composites with enhanced visible-light photocatalytic activity," *Journal of Nanoparticle Research* 729-736. DOI: 10.1007/s11051-007-9301-z
- Zhu, R. X., and Yu, W. J. (2010). "Effect of density on physical and mechanical properties of reconstituted small-sized bamboo fibrous sheet composite," *Advanced Materials Research* 150–151, 634-639. DOI: 10.4028/www.scientific.net/AMR.150-151.634
- Zhu, R., Zhang, Y., and Yu, W. (2015). "Outdoor exposure tests of bamboo-fiber reinforced composite: Evaluation of the physical and mechanical properties after two years," *European Journal of Wood and Wood Products* 73(2), 275-278. DOI: 10.1007/s00107-014-0873-x

Article submitted: April 21, 2017; Peer review completed: June 30, 2017; Revised version received and accepted: July 23, 2017; Published: August 1, 2017.
DOI: 10.15376/biores.12.3.6789-6811